Optics and Lasers in Engineering 202 (2026) 109773

Contents lists available at ScienceDirect

Optics and Lasers in Engineering

journal homepage: www.elsevier.com/locate/optlaseng

Planar validation of speckle pattern optimization for large-scale 3D streamlined structures in stereo digital image correlation using anamorphic transformation ⋆

Stéphane W. Hu [a,*], Guilhem Marchal [a], Yvan Dilem [a], Denis Walch [b], Ilyass Tabiai [a]

[a] Department of Mechanical Engineering, Ecole de Technologie Superieure (ETS), 1100 Notre-Dame St. W, Montreal, H3C 1K3, Quebec, Canada
[b] Advanced Structure, Bombardier, 1800 Marcel-Laurin Blvd., Saint-Laurent, H4R 1K2, Quebec, Canada

ARTICLE INFO

Keywords:
Digital image correlation
Anamorphic transformation
Speckle pattern optimization
Large objects viewed from tilted angles

ABSTRACT

This study addresses limitations of stereo Digital Image Correlation (DIC) when applied to large objects viewed from tilted angles (LOVTA), such as aircraft wings and fuselages. Under such configurations, perspective distortions lead to strong variations in apparent speckle size and spacing, which degrade correlation robustness and increase measurement uncertainty when conventional speckle patterns are used. To mitigate these effects, a geometric model is developed to generate anamorphic speckle patterns that explicitly pre-compensate for the known imaging geometry of the DIC setup. By locally transforming the reference pattern according to camera orientation and surface geometry, the proposed approach aims to maintain more uniform speckle characteristics in the image plane, thereby improving correlation conditioning.

An experimental comparison between regular and anamorphic speckle patterns is conducted on a planar target subjected to rigid-body rotations, under grazing-angle observation conditions representative of full-scale aircraft testing. The DIC analysis is used to extract the 3D positions of subset centers, from which uncertainty metrics are derived to assess correlation precision rather than to measure actual displacement or strain fields. The results show that the anamorphic speckle pattern consistently reduces matching uncertainty and improves the precision of 3D point localization compared to a regular pattern, even as camera incidence angles increase.

The study intentionally focuses on a controlled planar configuration to isolate perspective-induced effects and establish a clear baseline for validation. Although the transformation framework is formulated generically and illustrated analytically for curved surfaces, experimental validation of complex geometries and full-scale structures is identified as future work. The anamorphic transformation is applied offline during pattern generation and does not affect the DIC correlation workflow. Despite practical challenges related to pattern generation, application, and geometric modeling accuracy, the results demonstrate that geometric pre-compensation at the speckle-design stage is a promising and physically grounded strategy for reducing uncertainty in DIC measurements of large structures observed under strong perspective conditions.

1. Introduction

1.1. Background

The design, development, and validation of an aircraft prototype are divided into three main phases. The first phase is the design phase, during which the aircraft's characteristics and capabilities are defined to meet regulatory requirements. The second phase involves extensive ground testing, where all structural components and systems are evaluated using appropriate test rigs. The final phase is flight testing, where the complete aircraft is tested under real-world conditions.

A critical aspect of the design process is ensuring the mechanical integrity of the aircraft throughout these phases to prevent structural failures that could lead to major accidents. The mechanical behaviour of each component under various loads and conditions is thoroughly assessed through a series of tests [1,2]. Material testing to assess the basic mechanical properties such as strength, ductility, and fatigue life through tensile, compression, and fatigue tests. Static tests aim to verify that the newly designed structure can withstand the anticipated loads predicted by numerical simulations. For certification, the structure must remain in the elastic domain, avoiding permanent deformation under the designed limit load. Additionally, the structure must withstand loads

⋆ This document is the results of the research project funded by Bombardier and MITACS
* Corresponding author.
E-mail address: stephane.hu.1@etsmtl.net (S.W. Hu).

https://doi.org/10.1016/j.optlaseng.2026.109773
Received 10 November 2025; Received in revised form 11 March 2026; Accepted 30 March 2026
Available online 7 April 2026

up to the ultimate load, which is 150 percent of the designed limit load, without failure [1,2]. Structural failure should occur only beyond this ultimate load. Non-destructive testing is used to detect internal defects using methods like ultrasonic testing and radiography. Finally, environmental testing assesses the structure's performance under different conditions like temperature changes and corrosion.

The systematic method used to validate aircraft structures is the Building Block Approach (BBA) which consists of multilevel testing phases [3]. It begins with material characterization, testing basic material properties. This is followed by element testing, where simple structural elements are evaluated. Sub-component testing involves testing larger, more complex parts, while component testing assesses full-scale components. The final stage is full-scale testing, which validates the complete aircraft structure. The BBA offers several benefits. It helps mitigate risks by identifying and resolving potential issues early in the development process [3]. It is also cost-effective, as addressing problems at smaller scales is less expensive. The systematic validation ensures robust and reliable final products. Furthermore, it provides a structured path for demonstrating compliance with aviation safety standards [3]. Transitioning from the general framework of the BBA, it's essential to delve into the specific tools and techniques employed during the mechanical characterization tests in the next section. These standard characterization tools are pivotal in accurately assessing material properties, laying the groundwork for subsequent testing phases.

1.1.1. Standard characterization tools

Mechanical characterization of the aircraft structure involves various tools and techniques to assess material properties, structural integrity, and behaviour under different environmental conditions. Manufacturers mainly use strain gages, accelerometers, and load cells to monitor the strain and load of the structure itself [1,2,4]. Linear variable Differential Transformers (LVDTs) are employed to measure the displacement at a specific point of the structure under loading. The instrumentation tools employed during a mechanical test are numerous and each comes with its challenges: These tools are sensitive to environmental conditions such as temperature and humidity changes that affect their piezoelectric material [1,2]. These influences can affect the accuracy of the measurements, necessitating compensation techniques by employing additional temperature and humidity gages [1,4]. Furthermore, the installation of these tools is critical. Strain gages, accelerometers, and load cells need to be properly bonded to the surface under study to provide accurate readings [1,2,4]. LVDTs require a precise alignment between the core and the coils, and misalignment can cause measurement errors and reduced sensitivity [1,4]. In addition to the complexity of the installation, electrical noise, and interference need to be mitigated requiring proper signal conditioning and shielding cables [1,4].

Overall, the instrumentation of a full-scale structure can be tedious because of the numerous tools that need to be employed [1,5]. Each of these devices plays a critical role in mechanical characterization and comes with its own limitations and drawbacks that must be carefully managed through proper installation, calibration, environmental compensation, and signal conditioning to ensure accurate and reliable measurements [1,4]. These limitations highlight the need for complementary techniques to provide precise and comprehensive data. One such technique is Digital Image Correlation (DIC). DIC offers a non-contact, full-field approach to measuring displacement, thus overcoming many of the challenges associated with traditional tools. By leveraging high-resolution imaging and sophisticated software algorithms, DIC provides precise and extensive data that enhances the overall characterization of aircraft structures.

1.1.2. Digital image correlation

DIC is an optical, non-contact technique involving cameras to measure full-field measurement of an object's surface. A speckle pattern is applied to the specimen's surface. One digital camera (2D-DIC) or multiple cameras (3D-DIC or stereo-DIC) capture digital frames of the evolving speckle pattern applied to an object under mechanical loading. Subsequently, displacement fields are measured and strain fields are computed through a correlation algorithm by comparing the deformed speckle pattern with the reference one on each frame. Over time, DIC has gained popularity as a technique for conducting accurate full-field measurements in experimental mechanics ([6–10]).

DIC could be employed at all levels of the Building Block Approach (BBA) due to its versatility, accuracy, and comprehensive measurement capabilities. At the material characterization level, DIC allows for precise, non-contact measurement of material properties, reducing the risk of influencing material behaviour during testing. It provides full-field strain and deformation data, offering a comprehensive understanding of the material's response under various loading conditions ([7,9,11]). DIC is a widely used experimental technique for measuring deformation and strain fields in heterogeneous materials under tensile loads. It is also employed in compression testing to assess material behaviour under compressive forces. For fatigue testing, DIC analyzes material behaviour under cyclic loading, helping to predict fatigue life and failure points [12]. In fracture mechanics testing, DIC investigates crack initiation and propagation to understand fracture toughness and material durability [10]).

Moving to element testing, DIC captures strain distributions over the entire surface of simple structural elements, providing insights into localized deformations and potential stress concentrations that traditional tools might miss. Its high spatial resolution helps in identifying and analyzing small-scale features and defects within structural elements. For sub-component testing, DIC effectively measures strain and displacement in sub-components with complex geometries, which are often challenging to instrument with traditional sensors. It enables three-dimensional deformation measurements, crucial for accurately assessing the behavior of more intricate parts under load. When testing larger components, DIC can cover extensive areas without the need for multiple sensors, providing a comprehensive view of the component's structural response. DIC has been used in civil engineering for structural analysis of large structures like bridges. During full-scale testing, DIC can be used to simultaneously analyze global structural behavior and local detailed deformations, offering a holistic understanding of the aircraft structure. By reducing the need for extensive traditional instrumentation, DIC simplifies the setup and decreases potential sources of error related to sensor placement and environmental influences.

The advantages of using DIC at all levels of the BBA include its versatility, as it can be adapted to a wide range of test setups and structural scales, making it applicable across all BBA levels. The technique provides detailed, full-field data that enhance the understanding of structural behavior, improving the reliability of validation processes. As a non-contact method, DIC does not interfere with the test specimens, ensuring that measurements are not influenced by the presence of sensors. Moreover, DIC can streamline the testing process by reducing the need for multiple sensors and complicated setups, saving time and resources. By employing DIC at all levels of the BBA, manufacturers and researchers can achieve a more detailed, accurate, and comprehensive assessment of aircraft structures, ultimately leading to safer and more reliable aircraft designs.

1.1.3. Subset-based DIC

One of the most prevalent approaches is subset-based DIC as depicted in Fig. 1, which involves subdividing the Region of Interest (ROI) into subsets – sets of pixels within a square centred around a specific pixel ([8–11,13]). Consider an arbitrary pixel, denoted as i, with coordinates $\mathbf{x}$ in the reference image. In the deformed image, this pixel i undergoes displacement to a new position $\mathbf{X}$. Its relationship with the reference position is expressed as $\mathbf{X} = \mathbf{x} + \mathbf{u}$, where $\mathbf{u}$ represents the measured displacement vector. Let $g(\mathbf{x})$ and $G(\mathbf{X})$ represent the gray intensities of each pixel in the reference and deformed images, respectively.

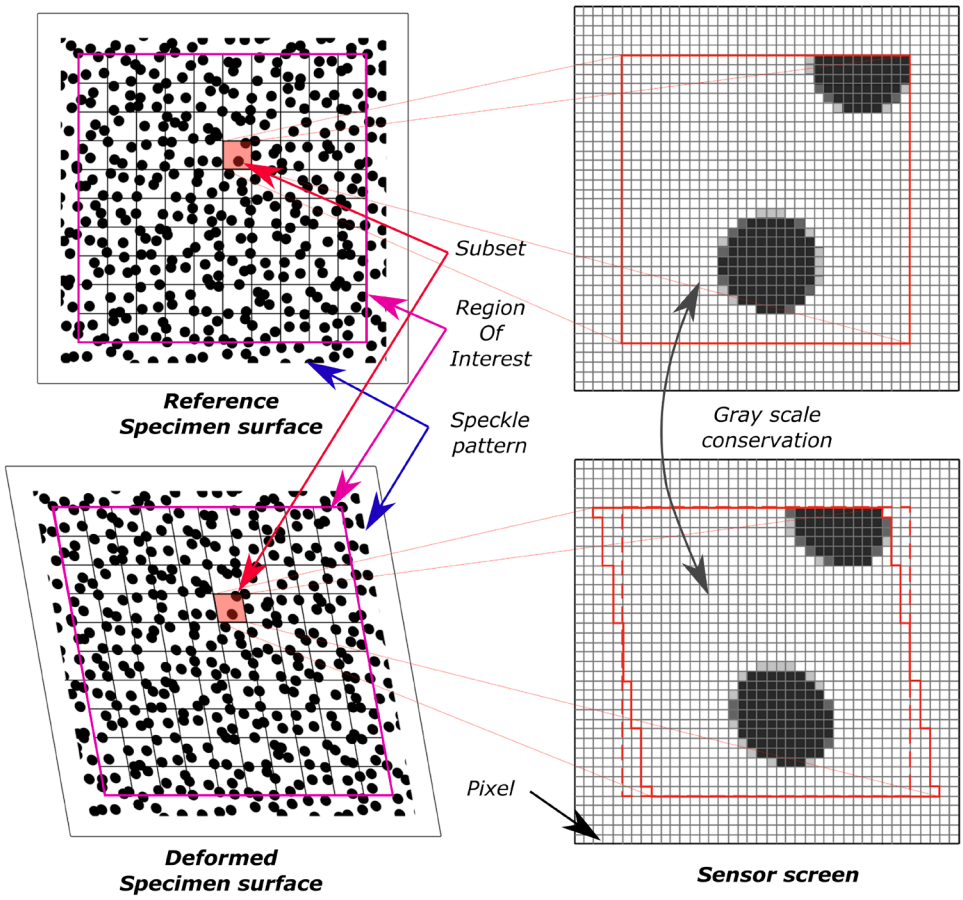

Fig. 1. Subset-based DIC method: The surface is partitioned into subsets within the region of interest. The grayscale within each subset is conserved during the deformation of the specimen.

Assuming the deformation is sufficiently small that the intensity pattern undergoes changes but not its local value, the relationship between the gray intensities in the reference and a deformed image is given by $G(\mathbf{X}) = g(\mathbf{x} + \mathbf{u})$. The displacement of each pixel can be ascertained by minimizing a correlation criterion C that defines how closely the grayscale intensities within two subsets on the reference and deformed images match each other. The minimization of C ensures that the deformed subset corresponds as closely as possible to the reference subset. The Sum of Square Difference criterion C_{SSD} articulated as follows is the sum of the squared differences between the pixel intensities of the reference and deformed subsets.

$$C_{SSD} = \sum [G(\mathbf{X}) - g(\mathbf{x})]^2 \tag{1}$$

Assuming that the measured displacement $\mathbf{u}$ and the time between the capture of the two images are small enough, $G(\mathbf{X})$ can be expanded as a first-order Taylor series expansion:

$$G(\mathbf{X}) = g(\mathbf{x} + \mathbf{u}) = g(\mathbf{x}) + \nabla g(\mathbf{x}).\mathbf{u} \tag{2}$$

Then, the C_{SSD} becomes:

$$C_{SSD} = \sum [\nabla g(\mathbf{x}).\mathbf{u}]^2 \tag{3}$$

The minimization of the correlation criterion is performed by calculating the inverse of the Hessian matrix $\mathbf{H}$ of the intensities [13].

1.2. Sources of uncertainty in DIC

DIC can be used to characterize the mechanical behaviour of 3D structures using two or more cameras positioned at different angles to capture images. A single camera setup can be used in some limited cases where the nature of the deformation is well understood as well as the geometry of the studied object. However, the most straightforward and reliable technique is to employ multiple cameras that must be synchronized and calibrated. Applications have already been made in the aerospace industry, showing great potential as a characterization tool ([14,15]).

The technique's greatest challenge at present is to obtain precise measurements over the entire surface of the structure under study [16]. The sources of uncertainty are diverse and can be classified into four main categories: optical defects, calibration errors, light intensity variations, and image-matching errors [16]. The combination of these errors leads to an uncertainty in the final 3D position of a measured point in space.

Regarding optical defects, lens distortion is one of the main sources of uncertainty due to manufacturing errors. Technological advances currently allow lenses to be manufactured with very low distortion rates [13]. However, it must be kept in mind that distortion will be more prevalent for larger fields of view. Regarding calibration errors, the main sources of error lie in the detection of the features of the calibration plate and the determination of its position in 3D from the cameras [17]. Work on this topic recommends that the calibration plate should cover at least 1/3 of the cameras' field of view to minimize this error ([13,17]). As far as light intensity is concerned, large variations can drastically distort DIC results by altering the pixel intensity from one image to the next. The C_{SSD} is directly impacted by such a sudden change in light intensity. On the other hand, other criteria exist such as the Normalized Sum of Squared Difference criterion C_{NSSD}, and the Zero-mean Normalized Squared Difference criterion C_{ZNSSD}. These enable the consideration of variations in lighting across different images, including a lighting offset

for the C_{NSSD} and both a lighting offset and scale for the C_{ZNSSD} [13]. This reduces the effects of light variation to the detriment of an increased calculation time [18].

Finally, the uncertainty on image matching has been extensively investigated by many researchers and is still an active research area ([16, 19–22]). This parameter is intrinsic to the DIC algorithm and is directly impacted by the light intensity and the speckle pattern itself. If the image sequence experiences illumination noise due to changes in ambient lighting, and the speckle pattern features are not clearly defined (as discussed in the following section), the measurements will exhibit a corresponding bias and variance in the image-matching process. Although it is hardly feasible to separate the impact of each factor, statistical analyses can be conducted to quantify them together by introducing independent Gaussian noises $\tau_1(\mathbf{x})$ and $\tau_2(\mathbf{X})$ of standard deviation σ into the intensities, representing intensity fluctuations in the reference and deformed images, respectively. Let $\mathbf{u}_0$, be the exact displacement vector, and $\mathbf{u'}$, the difference between the exact and measured displacement $\mathbf{u}$. Thus, the C_{SSD} in the Eq. (1) becomes:

$$C_{SSD} = \sum [g(\mathbf{x} + \mathbf{u}_0 + \mathbf{u'}) + \tau_2(\mathbf{X}) - g(\mathbf{x}) - \tau_1(\mathbf{x})]^2 \tag{4}$$

$$= \sum [g(\mathbf{x}) + \nabla g(\mathbf{x}).\mathbf{u'} + \tau_2(\mathbf{X}) - g(\mathbf{x}) - \tau_1(\mathbf{x})]^2 \tag{5}$$

$$= \sum [\nabla g(\mathbf{x}).\mathbf{u'} + \tau_2(\mathbf{X}) - \tau_1(\mathbf{x})]^2 \tag{6}$$

Let $\mathbf{u'} = [u'\ v']^T$, thus:

$$\frac{\partial C_{SSD}}{\partial u'} = 0;\ \frac{\partial C_{SSD}}{\partial v'} = 0$$

$$\Rightarrow \begin{bmatrix} u' \\ v' \end{bmatrix} = \mathbf{H}^{-1} \cdot \begin{bmatrix} \sum \tau_1(\mathbf{x}).\nabla g_x(\mathbf{x}) - \sum \tau_2(\mathbf{X}).\nabla g_x(\mathbf{x}) \\ \sum \tau_1(\mathbf{x}).\nabla g_y(\mathbf{x}) - \sum \tau_2(\mathbf{X}).\nabla g_y(\mathbf{x}) \end{bmatrix} \tag{7}$$

with $\mathbf{H}$, the Hessian matrix of the intensities:

$$\mathbf{H} = \begin{bmatrix} \sum [\nabla g_x(\mathbf{x})]^2 & \sum [\nabla g_x(\mathbf{x}).\nabla g_y(\mathbf{x})] \\ \sum [\nabla g_x(\mathbf{x}).\nabla g_y(\mathbf{x})] & \sum [\nabla g_y(\mathbf{x})]^2 \end{bmatrix}.$$

From the Eq. (7), the expectation and variance of the measured displacement $\mathbf{u}$ can be determined:

$$E(\mathbf{u}) = \mathbf{u}_0 \tag{8}$$

$$Var(\mathbf{u}) = 2\sigma^2.\mathbf{H}^{-1} \tag{9}$$

In this theoretical reconstruction of the error propagation performed by the DIC algorithm, there is a dispersion around the expected value of the displacement. An uncertainty of the measurement expressed in pixels $\sigma(\mathbf{u})$ can be approximated by calculating the square root of the variance $Var(\mathbf{u})$. $\mathbf{H}^{-1}$ can be approximated as the covariance matrix for the correlation algorithm[1] ([13]). The measured displacement expectation $E(\mathbf{u})$ is also unbiased with respect to the exact displacement. This is due to the assumption of small deformations so that $G(\mathbf{X}) = g(\mathbf{x} + \mathbf{u})$. However, in many engineering applications, this assumption is wrong and the algorithm as such can lead to a decorrelation of the results i.e. a loss of tracking on some subsets in the ROI [13]. To overcome this problem, the measured displacement can be approximated with interpolation methods by introducing shape functions $\zeta(\mathbf{x}, \mathbf{u})$ that transforms the pixel coordinates from the reference subset to the deformed one. Typical shapes of $\zeta(\mathbf{x}, \mathbf{u})$ are polynomial functions. A general guideline suggests that employing higher-order functions yields more accurate displacement results but comes at the cost of slower processing times [13]. As interpolation is an approximate solution method, corresponding biases are introduced into the measured displacement expectation $E(\mathbf{u})$.

This analysis of error propagation in the DIC algorithm underscores the importance of accurate displacement measurements: Small deformations require high precision in measuring displacements because even minor inaccuracies can lead to significant errors in the overall deformation analysis. If the displacement measurements are not accurate, the propagated error can distort the understanding of the material or structural behaviour under stress. The DIC algorithm operates under the assumption that the measured displacement expectation $E(\mathbf{u})$ is unbiased with respect to the exact displacement. Accurate displacement measurements are essential to meet this assumption and ensure the reliability of the results. In the presence of small deformations, the variance in displacement measurements $Var(\mathbf{u})$ can be relatively low. Accurate displacement measurements help in maintaining this low variance, thus minimizing the overall error in the displacement and strain calculations.

A crucial factor in achieving accurate displacement measurements is the quality of the speckle pattern applied to the specimen's surface. The quality of the speckle pattern affects the accuracy of displacement measurements because poor quality or improperly applied speckle patterns can introduce noise and inaccuracies into the DIC analysis. In the subsequent section, the intricacies of speckle pattern quality and its limitations in the context of displacement measurements will be detailed. Understanding these aspects is deemed crucial for optimizing experimental setups and enhancing the precision of DIC techniques in capturing and analyzing material deformations effectively.

1.3. Speckle pattern limitations for large objects

One of the most challenging steps in DIC is to apply an adapted speckle pattern in Fig. 2 to reduce image-matching errors. Indeed, its quality greatly impacts the precision of DIC measurements. It is assessed by its contrast, randomness, isotropy, and stability [23], each of these terms is defined as follows:

- High contrast: the variation of gray intensities should be large. Each feature should be clearly recognizable.
- Randomness: the pattern should be non-periodic and non-repetitive,
- Isotropy: the speckles should be uniformly distributed,
- Stability: the speckle pattern should adhere to the surface and deform with the specimen under loading to assess the mechanical properties.

Several manufacturing techniques exist to generate speckle patterns, each adapted to a specific scale. One approach is to use the material's natural texture as the feature for pattern matching, mainly at the microscale under controlled magnification. Otherwise, speckle patterns can be generated with airbrushing techniques, laser speckle patterns, spin coating, compressed air techniques, etc. [23].

Several studies have focused on optimizing speckle patterns at the micro- and meso-scale to improve measurement accuracy under challenging conditions. Li et al. (2023) [24] applied dense, high-contrast speckles on welding joints, with sizes tailored to subset dimensions to enhance strain resolution in localized microzones. Huang et al. (2023) [25] implemented bilayer color speckle patterns for liquid interfaces, using two distinct color layers to improve feature distinction in regions with low texture contrast. For high-speed rotating gears, Hou et al. (2025) [26] produced fine, uniform speckles with carefully controlled droplet size and spacing, enabling robust tracking with the SURF algorithm despite rotations and minor out-of-plane motion. These approaches show that speckle size, density, contrast, and color can be specifically designed to enhance correlation performance for small- to medium-scale measurements. However, these techniques are not intended for large surfaces.

With large objects at the macroscale, traditional speckle patterns become inadequate. The features are often smaller than a pixel and thus not clearly defined on the sensor, which is critical because DIC subdivides the region of interest into subsets. Correlated Solutions recommends the use of stamp rollers[2] to create a random distribution of black dots of a controlled size on a white-painted surface. Here, the diameter,

[1] https://correlated.kayako.com/article/60-vic-3d-9-manual-and-testing-guide

[2] https://www.correlatedsolutions.com/accessories-ref/speckle-kits

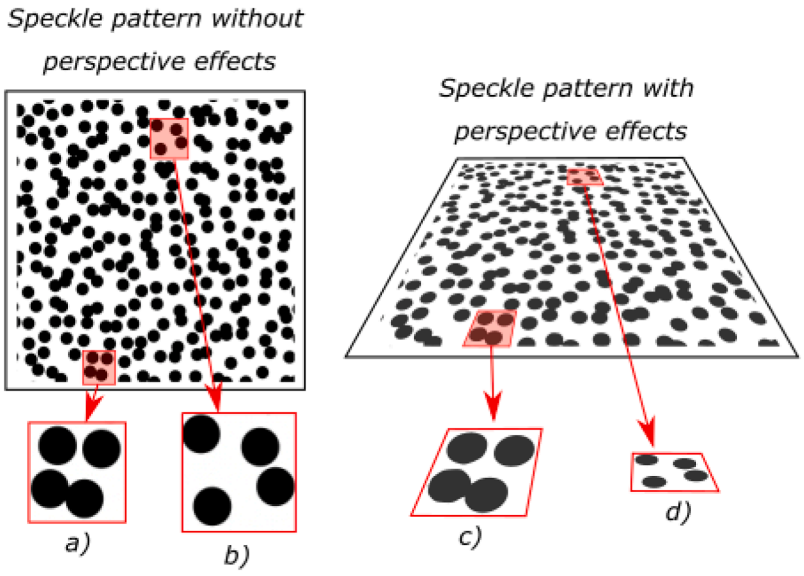

Fig. 2. Comparison between a speckle pattern with and without perspective effects. The one from the right is highly tilted with respect to the camera angle of view. The speckles in *a)* and *b)* have circular shapes and the same diameter. In *c)* and *d)*, the appearing dots are deformed and don't have the same size.

density, and randomness contribute to a quality speckle pattern. This method works when the object is at a fixed distance from the camera and the dots appear approximately the same size in the collected images.

However, depending on the shape of the object under study, it is not always possible to achieve an acceptable angle of view. In the context of the present work, "large scale" refers to measurement configurations typical of aeronautical structures, where the observation distance and the field of view are significantly larger than in conventional laboratory-scale DIC experiments. In such configurations, cameras observe the surface at large distances and often under oblique viewing angles, which amplifies perspective-induced distortions. Additionally, optical effects such as limited depth of field, lens distortion, and variations in apparent speckle size across the field of view further challenge accurate image correlation. If the surface of the object is highly tilted with respect to the camera–Large Objects Viewed from Tilted Angles (LOVTA)–the appearing speckle pattern will be strongly deformed as shown in Fig. 2. The dots lose their circular shape, and speckles furthest from the camera appear smaller than those closest. These perspective effects result in a loss of precision for areas of the surface far from the cameras, since the subsets are squared. In extreme cases, the speckles may be too small to be captured at a fixed sensor resolution.

Previous work on a small-scale composite wing using DIC illustrated these issues with the generation method proposed by Correlated Solutions [15]. Cameras with an oblique, low-angle view at the wing root exhibited a gradual loss of accuracy toward the wingtip. Li et al. (2014) [14] tried pre-stretched speckles to reduce perspective effects on large surfaces. While this approach partially compensates for distortions, it has limitations for LOVTAs. Speckles are printed as ovoids instead of circular dots to mimic a pre-stretched pattern, which works over short depth ranges with relatively uniform apparent speckle sizes. However, as depth variation increases, distant speckles appear distorted or differently sized, leaving residual perspective-induced errors that can affect DIC measurement accuracy. Pre-stretched speckles are thus effective for relatively flat surfaces but insufficient for complex or extensive structures where uniform speckle representation is critical.

1.3.1. Anamorphic transformation

This introduction aimed to describe the standard mechanical characterization methods of aerospace structures. These methods follow a BBA approach to validate all components of the aircraft at every scale rigorously. The standard instrumentation used to characterize these structures is complex in terms of installation, time, intrusiveness, and cost. Therefore, it is interesting to use other methods in conjunction with traditional equipment such as DIC. This method offers numerous advantages, and its operational principle is described. Various sources of uncertainty are introduced, and error propagation through the algorithm is explained. This serves to underscore the importance of a good speckle pattern to mitigate these uncertainties and achieve precise results. However, designing an optimal speckle pattern is challenging, especially for LOVTAs, where the issue primarily lies in the size of the points appearing in the image due to perceptual effects. In previous work, such as the study by Li et al. (2014) [14], pre-stretched speckle patterns were employed to partially compensate for perspective distortions. In this approach, ovoid speckles replace circular dots to mimic the effect of a pre-stretched pattern. While effective for short depth ranges and relatively flat surfaces, this method has notable limitations for LOVTAs. When the surface exhibits larger depth variations, speckles in distant regions still appear distorted, producing non-uniform apparent sizes. Consequently, perspective-induced errors are not fully eliminated, and the compensation effectiveness diminishes on complex or extensive structures.

An anamorphosis is a form of optical illusion that distorts an image so that it appears normal only when viewed from a particular viewpoint or with a special device [27]. This technique has been used historically in art and more recently in specialized media to create hidden images or illusions that only become clear when viewed from a particular angle or with a specific device, such as a mirror or lens. Anamorphosis has a rich history in art, dating back to the Renaissance and Baroque periods [27]. Artists like Leonardo da Vinci and Hans Holbein the Younger experimented with these techniques to create intriguing visual effects in their paintings. In modern times, anamorphosis has also been used in street art, where artists create large-scale illusions that interact with the urban environment and viewers.

Anamorphosis could offer significant benefits in mitigating perspective effects for speckle patterns by its ability to control visual perception. By intentionally distorting the speckle pattern according to the camera viewpoint, the anamorphic transformation ensures that the speckles appearing in the images maintain consistent size and distribution, even for large tilt angles or surfaces with depth variation. Unlike pre-stretched patterns, which are limited to small depth ranges, the anamorphic approach can compensate for varying distances across the measurement surface, preserving speckle isotropy, contrast, and randomness for reliable DIC tracking. Sanchez-Reyez et al. (2016) developed a

mathematical model to describe the principles of anamorphosis [27]. The goal of this study is to transform a reference speckle pattern using this mathematical model, effectively mitigating the perspective effects for LOVTA. The next sections of this paper will describe the application of the anamorphosis model to the speckle pattern. This will include a detailed comparison between a regular speckle pattern and an anamorphic speckle pattern, highlighting the differences and advantages of the latter. The experimental setup used to conduct this comparison will be thoroughly explained, along with the methods employed to evaluate and compare the performance of both speckle patterns. The results of these experiments will be presented, followed by a discussion that analyzes the findings. Finally, the paper will conclude with a summary of the key insights and implications of this work, emphasizing the potential benefits of using anamorphic transformations to enhance the precision of DIC measurements for LOVTA.

2. Methodology

A key challenge in this technique is creating an appropriate speckle pattern. For LOVTA, the existing design of speckle patterns may not be suitable. The concept driving this research involves employing anamorphic transformations to counterbalance the perspective effects arising from the orientation of the cameras.

In the present study, the experimental validation of the proposed approach is intentionally conducted on a planar target under controlled conditions. This configuration provides a well-defined reference case that allows perspective-induced effects to be isolated and the effectiveness of the anamorphic speckle transformation to be evaluated without additional geometric complexities. The objective of this work is therefore methodological: to establish the transformation framework and demonstrate its practical implementation in a controlled experimental setup.

This section details the process of applying this transformation to a regular speckle pattern. Following that, the approach for both qualitative and quantitative assessment of this transformation will be thoroughly outlined.

2.1. Anamorphic transformation of a speckle pattern

Fig. 3 illustrates a schematic of the anamorphic transformation ϕ, projecting a speckle onto a plane P_{Π} on an oriented developable surface S. Mathematically, ϕ can be described using homogeneous coordinates [27]. Consider a pinhole camera as the viewpoint in a 3D Euclidean space with origin O and axes $(\vec{x}, \vec{y}, \vec{z})$. Let M be a point with coordinates (x_M, y_M, z_M) on P_{Π}, and M' with coordinates $(x_{M'}, y_{M'}, z_{M'})$ be the projection of M on S. M and M' share the same projection on the sensor screen of the pinhole camera. Represent $\underline{M}$ with homogeneous coordinates as:

$$\underline{M} = \alpha \begin{bmatrix} M \\ 1 \end{bmatrix}, \text{ with } \alpha \neq 0.$$

The anamorphic transformation ϕ can be defined as follows:

$$\underline{M} = \alpha \begin{bmatrix} M \\ 1 \end{bmatrix} \xrightarrow{\phi} \underline{M'} = \alpha \begin{bmatrix} M \\ \delta \end{bmatrix} \longrightarrow M' = \frac{M}{\delta}, \tag{10}$$

with $1/\delta$, a dilatation factor being the unknown in this problem.

Let $s : R^3 \longrightarrow R$ be the characteristic equation of S:

$$M'(x_{M'}, y_{M'}, z_{M'}) \in S \Leftrightarrow s(x_{M'}, y_{M'}, z_{M'}) = 0.$$

The dilation factor $1/\delta$ is determined by substituting the projected point $M' = M/\delta$ into the surface equation $s(M') = 0$. For each point on the reference speckle pattern, this yields a scalar equation in δ, which can be solved numerically given the known surface S and the camera parameters defining the projection. By iterating this process for all points in the pattern, the complete anamorphic transformation is computed. This approach guarantees that, after transformation, each speckle point projects to the intended location on the imaging sensor according to the pinhole camera model. Knowing (10), δ can be found by solving:

$$s(M') = s\left(\frac{x_M}{\delta}, \frac{y_M}{\delta}, \frac{z_M}{\delta}\right) = 0. \tag{11}$$

2.1.1. Anamorphic transformation on a planar surface and a cylinder

2.1.1.1. Planar surface example. To illustrate how the dilation factor δ is computed in practice, consider a simple tilted planar surface. A generic plane can be described by the characteristic equation:

$$s(x, y, z) = ax + by + cz + d = 0, \tag{12}$$

where a, b, and c define the plane's normal vector, and d is the offset from the origin. For a speckle point $M = (x_M, y_M, z_M)$ in the reference pattern, the transformed point $M' = (x_{M'}, y_{M'}, z_{M'})$ satisfies:

$$M' = \frac{M}{\delta}. \tag{13}$$

Substituting M' into the plane equation gives:

$$s(M') = a\frac{x_M}{\delta} + b\frac{y_M}{\delta} + c\frac{z_M}{\delta} + d = 0, \tag{14}$$

which can be solved analytically for δ:

$$\delta = \frac{ax_M + by_M + cz_M}{-d}. \tag{15}$$

The transformed speckle coordinates are then:

$$M' = \frac{M}{\delta} = \left(-\frac{x_M d}{ax_M + by_M + cz_M}, -\frac{y_M d}{ax_M + by_M + cz_M}, -\frac{z_M d}{ax_M + by_M + cz_M}\right). \tag{16}$$

This provides a closed-form solution for the planar case, ensuring that each speckle projects correctly onto the plane as seen by the camera.

2.1.1.2. Cylindrical surface example.. As a simple curved surface, consider a generic cylinder described by:

$$s(x, y, z) = ax^2 + by^2 + cz^2 + dx + ey + fz + g = 0, \tag{17}$$

where the constants a, b, c, d, e, f, g define the cylinder's orientation, radius, and position. For a speckle point $M = (x_M, y_M, z_M)$, the anamorphic transformation projects it onto the cylinder surface as:

$$M' = \frac{M}{\delta} = \left(\frac{x_M}{\delta}, \frac{y_M}{\delta}, \frac{z_M}{\delta}\right). \tag{18}$$

Substituting M' into the cylinder equation:

$$a\left(\frac{x_M}{\delta}\right)^2 + b\left(\frac{y_M}{\delta}\right)^2 + c\left(\frac{z_M}{\delta}\right)^2 + d\frac{x_M}{\delta} + e\frac{y_M}{\delta} + f\frac{z_M}{\delta} + g = 0, \tag{19}$$

and multiplying through by δ^2 yields a quadratic equation in δ:

$$ax_M^2 + by_M^2 + cz_M^2 + (dx_M + ey_M + fz_M)\delta + g\delta^2 = 0. \tag{20}$$

Solving this quadratic gives:

$$\delta = \frac{-(dx_M + ey_M + fz_M) \pm \sqrt{(dx_M + ey_M + fz_M)^2 - 4\,g(ax_M^2 + by_M^2 + cz_M^2)}}{2g}. \tag{21}$$

The transformed coordinates are:

$$M' = \frac{M}{\delta} = \left(\frac{x_M}{\delta}, \frac{y_M}{\delta}, \frac{z_M}{\delta}\right), \tag{22}$$

ensuring that each speckle lies exactly on the cylinder surface.

These examples demonstrate that the anamorphic transformation can be applied to both planar and simple curved surfaces. By computing δ locally for each speckle based on the surface equation and point coordinates, the transformed pattern maintains the spacing, contrast, randomness, and isotropy of the speckles. This ensures that the resulting pattern remains suitable for stereo-DIC, reducing perspective-induced errors while preserving the essential qualities needed for accurate full-field measurements.

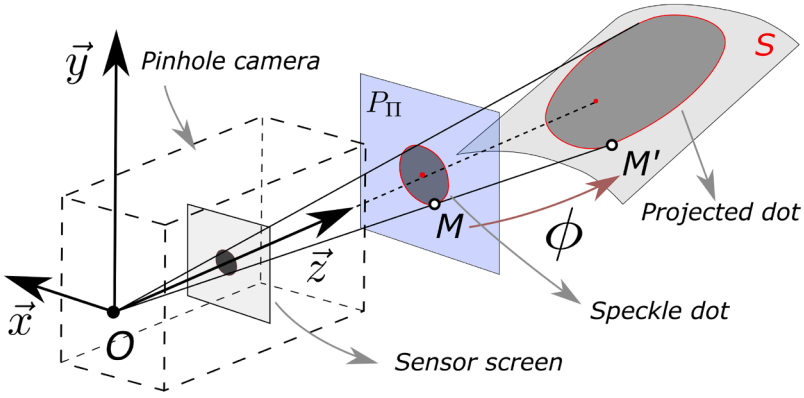

Fig. 3. Anamorphic transformation of a circular speckle projected onto a developable surface S: This illustrates how different points on the surface, such as M and M', project to the same location on the pinhole camera's sensor due to the anamorphic transformation.

Importantly, the effectiveness of this transformation relies on an accurate description of the imaging geometry. The anamorphic transformation is formulated within a pinhole camera model and therefore inherently depends on the intrinsic and extrinsic parameters defining the imaging geometry. The computation of the local dilation factor δ relies on the known camera pose and surface orientation used to project each speckle point onto the target surface. As in conventional stereo-DIC, accurate camera calibration is required to ensure consistency between the geometric model and the physical setup. The proposed approach does not introduce additional sensitivity to calibration errors beyond that already present in standard DIC measurements.

2.2. Practical generation of anamorphic speckle patterns

In summary, the anamorphic transformation maps each speckle point from the reference plane onto the target surface by computing a local scaling factor δ that ensures alignment with the camera viewpoint as shown in Fig. 3. For planar surfaces, δ has a closed-form solution, while for curved surfaces such as cylinders, it can be determined from a simple quadratic equation. This geometric mapping preserves the speckle pattern's essential properties, including contrast, randomness, and isotropy, ensuring accurate and reliable stereo-DIC measurements.

Creating an anamorphic transformation for any developable surface begins by digitally generating a reference 2D speckle pattern that is positioned on P_Π. This process can be executed using an available program[3] by specifying the diameter of the dots, their density, and randomness. This approach inherently produces a high-contrast speckle pattern with distinct black-and-white pixels. Choosing a clearly defined dot diameter minimizes speckle noise in the collected images. Dot density should ensure an even distribution of black and white pixels within the ROI. Subsequently, a Python script can identify the contour of each speckle using a specific function[4] from the OpenCV library. This yields a set of points representing each dot's discrete perimeter. Each point is then projected onto the target surface S by solving Eq. (11), where S is defined by its characteristic equation $s(x, y, z) = 0$. This equation can represent a planar surface, a cylinder, or any developable geometry, allowing the computation of the local dilation factor δ that maps the reference speckle to the surface as seen by the camera.

The same geometric projection principle can be extended to curved surfaces, such as aircraft wings, fuselages, or other complex aeronautical structures. When the surface geometry is known, either analytically or through a measured 3D mesh, the anamorphic transformation can be applied point by point by projecting the speckle coordinates along the camera viewing direction until intersection with the surface, from which the local dilation factor is computed based on the surface normal and camera incidence. This procedure ensures that speckle size and spacing are preserved in the image, maintaining essential properties such as contrast, randomness, and isotropy across the surface.

In practical applications where an explicit surface equation may not be available, the same principle can be implemented using CAD models of the structure. In this case, the reference speckle pattern is mapped onto the digital geometry, and the local orientation and position of each surface element are used to compute the corresponding projection of the speckle points. This approach enables the generation of anamorphic speckle patterns for highly complex or free-form surfaces, while relying on the same underlying geometric framework as the planar and analytically defined cases. The detailed implementation of this strategy, including CAD-to-physical mapping and associated sources of uncertainty, will be addressed in future work.

2.3. Experimental setup

To study the potential benefits of the anamorphic transformation, an anamorphic speckle pattern (SP-2) is generated using the previous Python package on a tilted plane at 70°. As illustrated in Fig. 4, a reference plane (SP-Ref) is positioned 2.5 m away from a stereo camera device that will be detailed in the next section. Another plane (SP-1 and SP-2) of 1.2m long, is tilted at various angles $\theta = \theta_{ref} + \theta'$ with θ_{ref}, the initial angle between the reference and the tilted planes, and θ', angular increments of 2.5°. SP-Ref and SP-1 are regular speckle patterns with 2mm dots, chosen for clear identification based on camera resolution and positioning. Stereo images will be acquired of each θ creating an image sequence from θ_{ref} to θ_f for DIC analysis, with θ_f the final angle between the reference and tilted planes.

For this study, the simple case of a planar surface has been selected. The planar setup is straightforward to implement experimentally, allowing precise control of the tilt angle, alignment, and camera positioning, which facilitates (repeatable maybe) measurements. Moreover, it provides a clear illustration of the anamorphic transformation principle without introducing additional geometric complexities. This setup also approximates the point of view of a camera placed in the cabin of an aircraft observing a wing, with the wing modeled as a planar surface. Although this is a simplifying assumption, it still provides significant benefits by validating the transformation under realistic viewing conditions. This approach has the advantage of generating a well-defined reference for validating the method.

2.3.1. Image acquisition

Two monochrome CCD cameras, Grasshopper 3-51SM5M, will be utilized to capture images with a resolution of 2048x2448 pixels. As shown in Fig. 5: Exp setup, the cameras are mounted on a stereo support fixed to a tripod. The stereo angle between the cameras is adjustable

[3] https://www.correlatedsolutions.com/downloads
[4] https://docs.opencv.org/4.x/d4/d73/tutorial_py_contours_begin.html

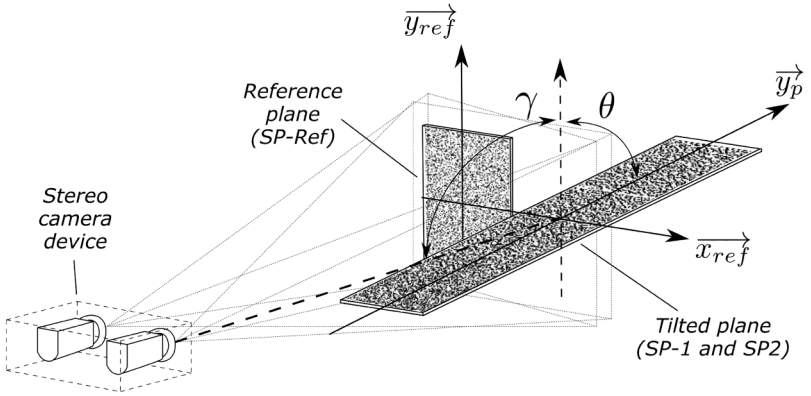

Fig. 4. Setup scheme: Two planes are tilted at an angle θ. Two cameras are placed at a fixed distance from the reference plane. A regular speckle SP-Ref is positioned on the reference plane. A regular (SP-1) and an anamorphic speckle pattern (SP-2) are positioned on the tilted plane.

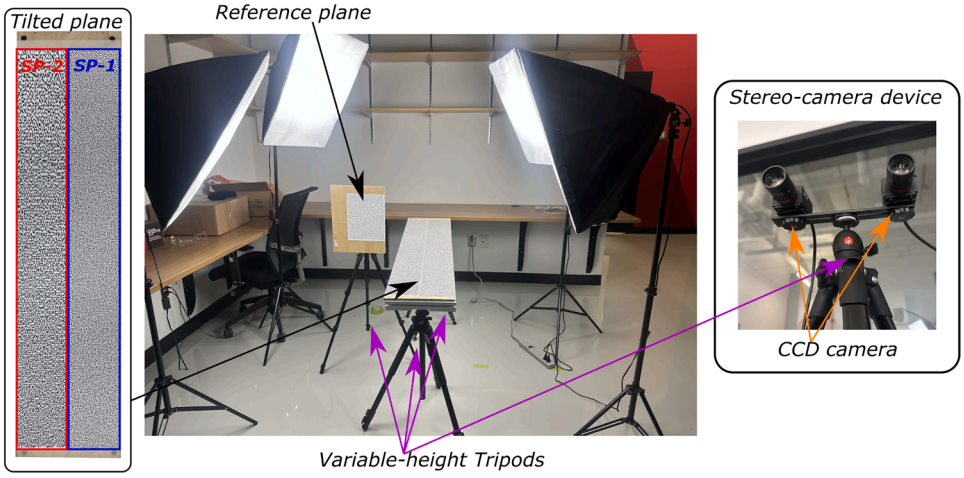

Fig. 5. Physical setup of the experiment: Wooden boards supported by variable-height tripods are used as adjustable planes, with printed speckle patterns attached to the boards. This arrangement allows for controlled variation of the plane orientations and distances.

to ensure proper convergence on the same point in space. The speckle patterns SP-ref, SP-1, and SP-2 are printed at actual size on sheets and then affixed to wooden boards. These boards, in turn, are mounted on variable-height tripods using 3D-printed fixtures. The angle θ between the boards is adjusted by varying the height of the tripods and can be accurately measured with a protractor and a digital inclinometer to the nearest tenth of a degree. Four spotlights are positioned on both sides of the wooden boards to enhance the lighting of the scene. Experiments were conducted under these controlled illumination conditions using a large photographic LED panel, as shown in Fig. 5. Due to the proximity of SP-ref and SP-2, minor shadowing naturally occurs in certain areas; however, this does not compromise the global uncertainty metrics used to compare the performance of SP-2 with SP-ref. The impact of lighting on DIC measurements has been thoroughly investigated in a complementary study on in-flight DIC, where advanced imaging and illumination strategies are implemented to mitigate shadowing and ensure robust measurements under complex real-world conditions. A set of collected images with SP-1 and SP-2 is acquired for different θ values with $\theta_{ref} = 74.7°$ with 2.5° increments: +2.5°, +5.0°, +7.5°, +10.0°, +12.5°, and +15.0°. In this instance, θ varies from 74.7° to 89.7°.

2.4. Influence of the camera incidence

Achieving the correct tripod height for various angles proved challenging. Maintaining precise angles and alignment of the inclined plane with its reference position complicated the experiment replication.

Accurately placing a camera at the anamorphosis origin is also difficult. In industrial settings, estimating camera positions depends on structure size, available space, and camera specifications. An anamorphic transformation can then be calculated based on this theoretical position. However, discrepancies will always exist between the actual and estimated camera positions. Therefore, investigating the cameras' inclination angle γ with a previously established anamorphic transformation becomes essential.

To address this, a DIC analysis can be conducted in a virtual environment, allowing for the precise fixation of the cameras' exact position relative to the reference plane. The experiment will be designed to be repeatable, facilitating the comparison of results across multiple tests. A quantitative comparison of DIC results between virtually generated and real images is not meaningful. In one scenario, the lighting conditions, camera alignment, and the angle between the reference plane and the tilted plane are optimal.

SolidWorks can generate virtual images. Multiple cameras can be placed in a space to capture views of an assembly. Various parameters, such as the field of view and resolution of the captured images can be defined. To mimic the real-world experiment, two inclined planes with an angle θ were created with the same dimensions as shown in Fig. 6. The cameras were precisely positioned at a distance of 2.5m from the reference plane. Their height and alignment were set to resemble the images collected in the real scenario closely. As for the virtual cameras, a field of view of 10.2° and a sensor resolution of 2048x2448 pixels were defined to match the specifications of the Grasshopper cameras

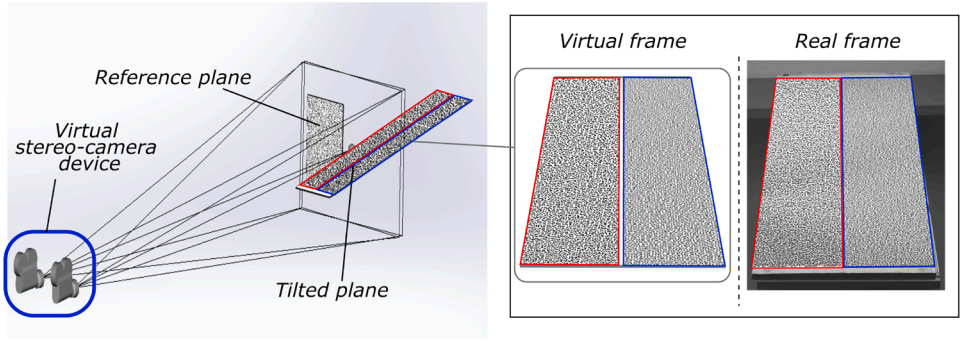

Fig. 6. Virtual setups for DIC. Left: virtual frame in SolidWorks captured by the virtual camera. Right: physical frame captured by real cameras.

closely. The *Decal*[5] and *Photoview 360*[6] options were utilized to paste digital speckle pattern layers onto the planes and generate virtual frames collected by the cameras for different angles θ.

2.5. DIC analyses

This section describes the methodology for characterizing speckle patterns, evaluating the two types of speckle patterns, and post-processing the collected results. VIC3D by Correlated Solution serves as the software for analyzing the acquired images. With user-friendly features, this software facilitates stereo-DIC analyses through the importation of calibration and experiment images. For stereo-calibration, the software provides a tool to derive intrinsic and extrinsic camera parameters by specifying the calibration plate's geometry The DIC analysis includes a graphical interface for selecting ROIs on the reference image and adjusting parameters like subset size and step. The algorithm provides a variety of correlation criteria, including C_{SSD}, C_{NSSD}, and C_{ZNSSD}, along with diverse interpolation options like *optimized 4-tap*, *optimized 6-tap*, and *optimized 8-tap*. As mentioned previously, the correlation criterion selection minimizes the influence of lighting. In this study, all of the DIC analyses are performed with the C_{ZNSSD} and an *optimized 8-tap* interpolation.

Concerning subset size, numerous applications have demonstrated that larger subsets contribute to reducing uncertainty in DIC measurements. This can be explained by considering that a larger subset contains more speckle features, which aids image matching. However, increasing subset size reduces correlation resolution, smoothing results in areas with strong deformation gradients. The step size is another parameter that determines the spacing between subset centers where correlation is performed. For example, a 1-pixel step size results in correlation analysis at every pixel in the ROI. Alternatively, a 10-pixel step size causes the algorithm to skip 9 pixels horizontally and vertically before analyzing the 10th pixel. Increasing step size significantly reduces processing time; for example, a 10-pixel step size is 10 times faster than a 1-pixel step size. However, this reduces the number of analyzed pixels, resulting in a less detailed correlation. Regarding the subset size and step, a step of $1/3$ of the subset size was fixed to obtain at least 3 independent data points for each subset. The various parameters are listed in the Table 1.

To evaluate the quality of the speckle patterns, one approach involves extracting the uncertainty in image matching by computing $Var(\mathbf{u})$. This metric provides a direct measure of the intrinsic precision of the correlation process: because the present experiments involve rigid-body motion with no physical deformation, any measured displacements arise solely from the DIC system's intrinsic noise, including effects of lighting, speckle quality, or calibration. VIC-3D offers a corresponding

Table 1
DIC parameters used for the assessment of the speckle pattern qualities.

Criterion	Interpolation	Subset size (pixel)	Step size (pixel)
C_{ZNSSD}	*Optimized 8-tap*	9	3
C_{ZNSSD}	*Optimized 8-tap*	15	5
C_{ZNSSD}	*Optimized 8-tap*	21	7
C_{ZNSSD}	*Optimized 8-tap*	27	9
C_{ZNSSD}	*Optimized 8-tap*	33	11
C_{ZNSSD}	*Optimized 8-tap*	39	13
C_{ZNSSD}	*Optimized 8-tap*	45	15
C_{ZNSSD}	*Optimized 8-tap*	51	17

parameter known as σ_{pixel}, allowing the quantification of match uncertainty for each subset center along the ROI. The software also furnishes similar parameters, namely $\sigma_X[mm]$,[7] $\sigma_Y[mm]$, and $\sigma_Z[mm]$, the 1-standard deviation uncertainty along the X, Y, and Z axes in millimetres that are obtained from σ_{pixel} via a triangulation algorithm - given the stereo angle and lens magnification. This enables the generation of full-field maps to assess correlation accuracy across the ROI of either speckle pattern (SP-1 or SP-2). From these, the computation of the mean uncertainty value in pixels and metrics with its standard deviation along the ROI for each θ angle position can be performed. Importantly, a low σ_{pixel} in this rigid-body configuration indicates that the correlation algorithm can reliably track subset positions with high precision. This baseline precision is critical because it sets the achievable accuracy for subsequent deformation measurements: the smaller the σ_{pixel}, the more sensitive the system is to small displacements or strain fields in real structural testing. Demonstrating low σ_{pixel} therefore provides strong evidence that the anamorphic speckle pattern enables precise and robust DIC tracking, supporting reliable deformation results in future experiments.

Following DIC analyses on SP-1 and SP-2, the 3D positions of subset centers are determined, enabling further calculations. The question arises as to whether SP-2 still produces comparable measurement results to SP-1 while reducing the uncertainty for the match. To explore this, all points on SP-1, or SP-2 can be fitted with a best-fit plane using a least squares method. This involves finding the plane that minimizes the sum of the squared distances between the measured data points and an ideal plane itself.

It should be emphasized that no physical deformation is applied to the targets in this study. The DIC analysis is therefore used solely to extract the 3D positions of subset centers and compute uncertainty metrics. This controlled approach allows assessment of the precision and repeatability of the correlation, isolating the effect of the speckle pattern and the anamorphic transformation on measurement

[5] https://help.solidworks.com/2021/english/SolidWorks/sldworks/t_Adding_a_Decal.htm
[6] https://help.solidworks.com/2020/english/SolidWorks/sldworks/c_photoview_360.htm
[7] https://correlated.kayako.com/article/60-vic-3d-9-manual-and-testing-guide

Table 2
DIC parameters analysis.

Subset size (pixel)	Mean σ_{pixel} SP1	Standard deviation SP1	Mean σ_{pixel} SP2	Standard deviation SP2
9	0.0240	0.000109	0.0296	0.000172
15	0.0126	0.000058	0.0114	0.000040
21	0.0087	0.000040	0.0074	0.000025
27	0.0067	0.000031	0.0056	0.000019
33	**0.0055**	**0.000025**	**0.0045**	**0.000015**
39	0.0046	0.000021	0.0038	0.000012
45	0.0040	0.000019	0.0032	0.000011
51	0.0035	0.000016	0.0028	0.000010

uncertainty, which establishes a necessary baseline before performing deformation tests.

2.5.1. Evaluation of DIC parameters

Previously, it has been mentioned that the choice of subset size involves a compromise between spatial resolution in displacement and measurement noise: A finer discretization is achieved with a smaller subset, leading to a greater number of independent measurement points on the ROI. However, reducing this size also results in the introduction of noise and an increase in uncertainty for the match σ_{pixel}. To determine the appropriate subset size, the proposed method entails capturing multiple images of the setup without applying any load. These images remain unaffected by displacement or deformation. DIC analysis can then be performed on these images to ascertain the average uncertainty for the match $\bar{\sigma}_{pixel}$ on the ROI for each parameter. In this scenario, a set of 8 successive images is taken at the reference position. The $\bar{\sigma}_{pixel}$ and its fluctuation σ' are calculated for each ROI for SP-1 and SP-2 with the parameters. Table 2 shows $\bar{\sigma}_{pixel}$ and its standard deviation for each subset size. Average uncertainty decreases nearly tenfold when transitioning from a subset size of 9 to 51. From a subset of 33 pixels onwards, the values flattens significantly. For all subset sizes from 15 to 51 pixels, the average uncertainty is lower for SP-2 than SP-1. However, in the case of a 9-pixel subset, SP-2 exhibits higher uncertainty. This is likely due to the larger appearance of points resulting from the anamorphic transformation. Below a certain threshold, the anamorphic transformation increases the likelihood of matching and uniqueness issues. Therefore, a subset size of 33 pixels has been chosen for the DIC analyses.

3. Results

The results presented in this section aim to quantify the impact of the proposed anamorphic speckle pattern on the accuracy and reliability of DIC measurements under perspective effects. The analysis is structured to progressively link speckle pattern characteristics to measurement performance. First, the intrinsic quality of the regular and anamorphic speckle patterns is assessed through grayscale histogram analysis, providing an objective comparison of contrast and intensity distribution. The influence of these properties on the matching uncertainty at the pixel level is then examined across the tested angular configurations. Subsequently, the propagation of matching uncertainty into metric uncertainties along the X, Y, and Z directions is evaluated. The overall spatial consistency of the reconstructed 3D data is further assessed through best-fit plane analysis. Finally, the sensitivity of the measurements to camera incidence is investigated using virtual image generation. Together, these results provide a comprehensive evaluation of the benefits and robustness of the anamorphic transformation for improving DIC performance under challenging geometric and optical conditions.

3.1. Quality assessment of regular and anamorphic speckle patterns

The quality of speckle patterns is a key factor influencing the accuracy of DIC measurements, as it affects the algorithm's ability to reliably track displacements. In this study, the speckle patterns were evaluated by analyzing grayscale histograms computed over carefully selected ROIs. Histograms provide a quantitative measure of intensity variation and contrast, which are critical for distinguishing features and ensuring robust subset matching under challenging imaging conditions. This assessment provides a basis for understanding how speckle quality can influence the precision of DIC measurements.

The speckle patterns were evaluated for their suitability in DIC measurements by analyzing selected ROIs for both the regular and anamorphic patterns, as shown in Fig. 7. Grayscale histograms were computed over these ROIs to quantify intensity variation and overall contrast. The regular pattern is represented in blue, while the anamorphic pattern is shown in red. The histograms indicate that the anamorphic pattern exhibits higher contrast, spanning a wider range of intensity values. This increased contrast improves feature distinguishability under perspective distortions, supporting more reliable subset matching during DIC analysis.

The improved grayscale properties observed in the anamorphic pattern, namely the higher contrast and broader intensity range, enhance the ability of the DIC algorithm to resolve individual features within each subset. This increased feature distinction reduces random matching errors, which directly contributes to reduced overall measurement uncertainties. The impact of these improvements on DIC accuracy and precision will be quantitatively analyzed in the following sections.

3.2. Uncertainty for the match

All experimental images, calibration data, and post-processed CSV files used in this study are openly available in a Zenodo repository [8]. In Fig. 8, the progression of uncertainty in the match σ_{pixel} is illustrated across various θ positions. The outcomes are shown using a subset of 33. The red and blue contours represent SP-2 and SP-1, respectively. The mean $\bar{\sigma}_{pixel}$ is calculated for all θ positions across the ROIs of SP-1 and S-P2. Fig. 8 plots its evolution. The error bars depicted in black represent the range $\left[\bar{\sigma}_{pixel} - Std, \bar{\sigma}_{pixel} + Std\right]$, with Std is the standard deviation of σ_{pixel} calculated using the Numpy[9] library. As the angle $\theta = \theta_{ref} + \theta'$ between the tilted plane and the cameras increases, there is a corresponding rise in uncertainty, denoted by σ_{pixel}, across the ROIs.

For SP-1, the mean value $\bar{\sigma}_{pixel}$ increases from 0.0054 to 0.0194. This signifies decreased precision in the DIC results as the tilted plane inclines further. This is expected due to perspective effects, which make the speckle pattern features appear progressively smaller in the images. The standard deviation Std, ranging from 0.0054 to 0.0194, reveals a progressively widening uncertainty along SP-1. At the last increment +15.0°, σ_{pixel} exhibits a notable decrease at the start of the plane compared to its value at the end.

An improvement is observed for the anamorphic speckle pattern SP-2, characterized by an overall lower σ_{pixel}, ranging from 0.0045 to 0.0132. The uncertainty is notably lower with the anamorphic speckle pattern, being 1.20 times better at the increment +0.0° and 1.46 times better at the increment +15.0°. The standard deviation of SP-2 ranges from 0.0008 to 0.0014, demonstrating a mild dispersal of σ_{pixel} over SP-2. Notably, an increase in σ_{pixel} is discernible in the dashed area, attributed to a shadow cast by the orientation of the light and the reference plate.

3.3. Uncertainties in X, Y, and Z axes

This effect on σ_{pixel} influences the overall precision of the metric measurement. Each subset center position is linked with uncertainties σ_X, σ_Y, and σ_Z derived from σ_{pixel} using the triangulation algorithm. Fig. 9 illustrates their distributions corresponding to the last increment +15.0°. Mean values of σ_X, σ_Y, and σ_Z along with their standard deviations $Std_{[mm]}$ are plotted for all θ positions. A progressive decline in precision is evident along the inclined plane.

[8] **DOI:** 10.5281/zenodo.17100439
[9] https://numpy.org/doc/stable/reference/generated/numpy.std.html

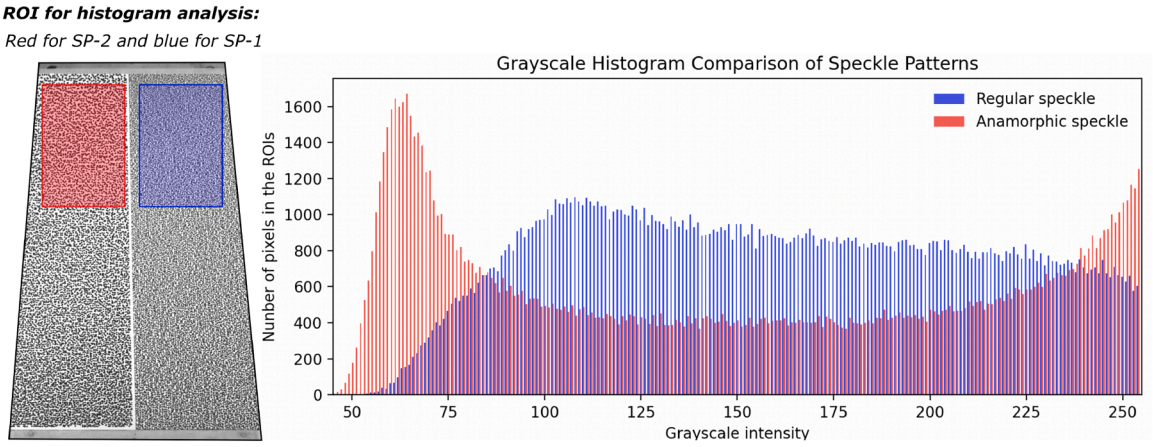

Fig. 7. Comparison of regular and anamorphic speckle patterns. The ROIs used to compute the histograms are highlighted, and the grayscale histograms show that the anamorphic pattern has higher contrast, although the distribution of intensities is less uniform than that of the regular pattern. The regular speckle pattern is shown in blue, the anamorphic one in red.

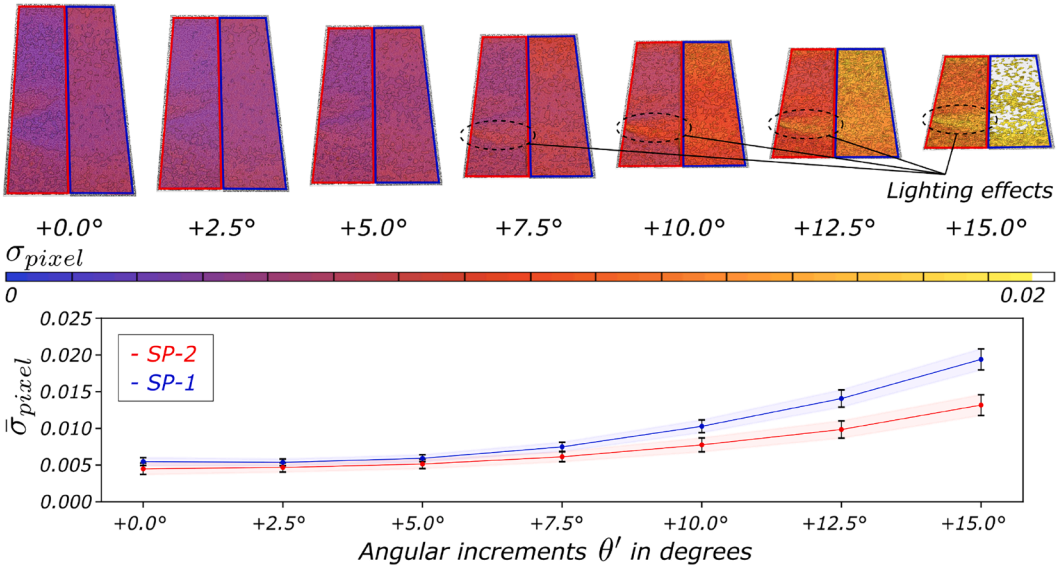

Fig. 8. Evolution of σ_{pixel} on SP-1 and SP-2 across all $\theta = \theta_{ref} + \theta'$ with a subset of 33 and $\theta_{ref} = 74.7°$: Blue and red contours indicate the ROIs of SP-1 and SP-2, respectively. The graphic below represents the mean value $\bar{\sigma}_{pixel}$ with its standard deviation for both speckle patterns. Across all θ positions, σ_{pixel} for SP-1 significantly higher than of SP-2. An increase in σ_{pixel} is observable in the dashed area, attributed to a shadow cast by the orientation of the light and the reference plane.

For SP-1, the uncertainties increase from 0.0108 to 0.0400 mm for σ_X, 0.0117 to 0.0415 mm for σ_Y, and 0.0122 to 0.0443 mm for σ_Z. Across all three axes, the uncertainties quadruple between the initial position $\theta = 74.7°$ and $\theta = 89.7°$. Additionally, the uncertainties become increasingly dispersed, with a standard deviation $Std_{[mm]}$ ranging from 0.0021 to 0.0087 mm for σ_X, 0.0027 to 0.0084 mm for σ_Y, and 0.0025 to 0.0096 mm for σ_Z.

Conversely, for SP-2, significant improvement is observed. σ_X varies from 0.0076 to 0.0233 mm, σ_Y from 0.0070 to 0.0209 mm, and σ_Z from 0.0075 to 0.0230 mm. Furthermore, the spread of uncertainties is narrower, with $Std_{[mm]}$ ranging from 0.0010 to 0.0042 mm for σ_X, 0.0011 to 0.0035 mm for σ_Y, and 0.0010 to 0.0040 mm for σ_Z.

For a clearer visualization of the impact of perspective effects on the uncertainties along the ROIs, Fig. 10 illustrates σ_X, σ_Y, and σ_Z along the vertical pixel coordinates across the image y_{pixel} at +15.0°. The ROIs for SP-1 and SP-2 begin at $y_{pixel} = 0$ and end at $y_{pixel} = 1441$ and $y_{pixel} = 1449$, respectively. The solid lines depict the mean uncertainties for each y_{pixel} value with their standard deviation along the x_{pixel} axis.

These results demonstrate a substantial difference in uncertainties between SP-1 and SP-2. For SP-1, σ_X increases from 0.0286 mm to 0.0517 mm, σ_Y from 0.0311 mm to 0.0552 mm, and σ_Z from 0.0320 mm to 0.0588 mm. The perspective effects lead to an almost linear evolution of uncertainties along the ROI. For SP-2, σ_X increases from 0.0192 mm to 0.0369 mm, σ_Y from 0.0179 mm to 0.0329 mm, and σ_Z from 0.0190 mm to 0.0363 mm. A localized increase is observable between $y_{pixel} = 250$ and $y_{pixel} = 550$ due to the shadow effect caused by the reference plane. Otherwise, the anamorphic transformation helps mitigate the perspective effects, maintaining uncertainties almost constant until $y_{pixel} = 1100$, where they start to rise.

3.4. Spatial positioning of the data points

The preceding sections were dedicated to illustrating a marked enhancement in uncertainty for the match σ_{pixel}, particularly evident with the anamorphic speckle pattern SP-2, and its consequent effect on uncertainties along the X, Y, and Z axes. To comprehensively gage the impact on DIC measurements, the entire set of 3D coordinates for subsets corresponding to each speckle pattern, SP-1, and SP-2, can be interpolated and assessed using a least squares method to derive a best-fit plane with

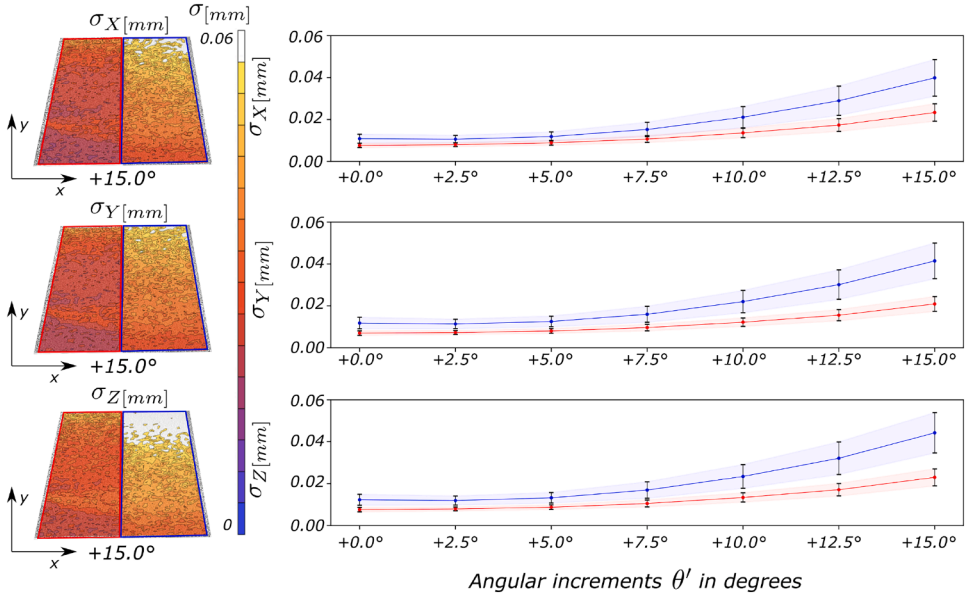

Fig. 9. Distribution of σ_X, σ_Y, and σ_Z on SP-1 and SP-2 at the last increment +15.0° with a subset of 33. Their mean values are plotted for all angular increments: The uncertainties along the axes x, y, and z are greater for SP-1. A gradual increase in uncertainties is observable along the ROIs.

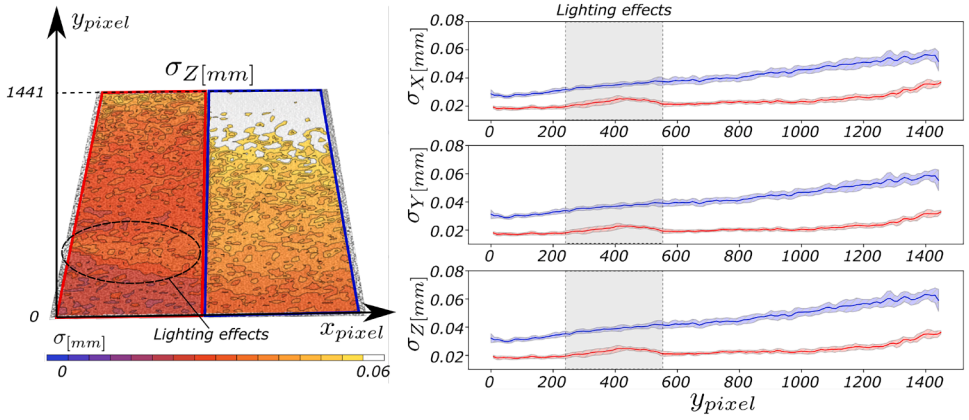

Fig. 10. Distribution of σ_X, σ_Y, and σ_Z on SP-1 and SP-2 at the final position of $\theta = 89.7°$ with a subset of 33 along y_{pixel}: The uncertainties along the axis x, y and z increase almost linearly along the ROI for SP-1. For SP-2, The uncertainties out-of-the lighting effect zone remain almost constant until $y_{pixel} = 1100$.

Table 3
Correlation coefficient for all interpolations.

Angular increment	R^2 SP1	R^2 SP2
+0.0°	0.9999	0.9999
+2.5°	0.9999	0.9999
+5.0°	0.9999	0.9999
+7.5°	0.9999	0.9999
+10.0°	0.9999	0.9999
+12.5°	0.9999	0.9999
+15.0°	0.9890	0.9928

the Scipy[10] library. All interpolations for both speckle patterns resulted in a correlation coefficient of $R^2 = 0.99$, as shown in Table 3. Overall, approximating the results with a best-fit plane is appropriate. SP-2 shows a slight improvement in R^2 at the last increment.

[10] https://docs.scipy.org/doc/scipy/reference/generated/scipy.optimize.lsq_linear.html

Fig. 11 showcases the 3D plot of data points from SP-1 depicted in blue and SP-2 in red, capturing both the +0.0° and +15.0° increments. The gray points signify those from SP-ref. Additionally, a plan view at $X = 400$ mm for SP-1 and $X = 300$ mm for SP-2 is provided, accompanied by the standard deviation illustrating the deviation of each point from the best-fit plane. Notably, SP-2 shows a substantial improvement, with a standard deviation half that of SP-1. Specifically, the standard deviation values for SP-1 are 0.19 mm for the +0.0° increment and 0.18 mm for the +15.0° increment. In contrast, for SP-2, these values are reduced to 0.10 mm for the +0.0° increment and 0.11 mm for the +15.0° increment.

3.5. Influence of the camera incidence

The precision of DIC measurements is influenced not only by speckle pattern quality but also by the relative orientation of the camera and the surface. In this section, the impact of camera incidence on measurement uncertainties is analyzed, and the robustness of the anamorphic speckle pattern SP-2 under variations in plane tilt and imaging conditions is evaluated. This assessment demonstrates how deviations from the reference configuration affect σ_{pixel} and highlights the flexibility of

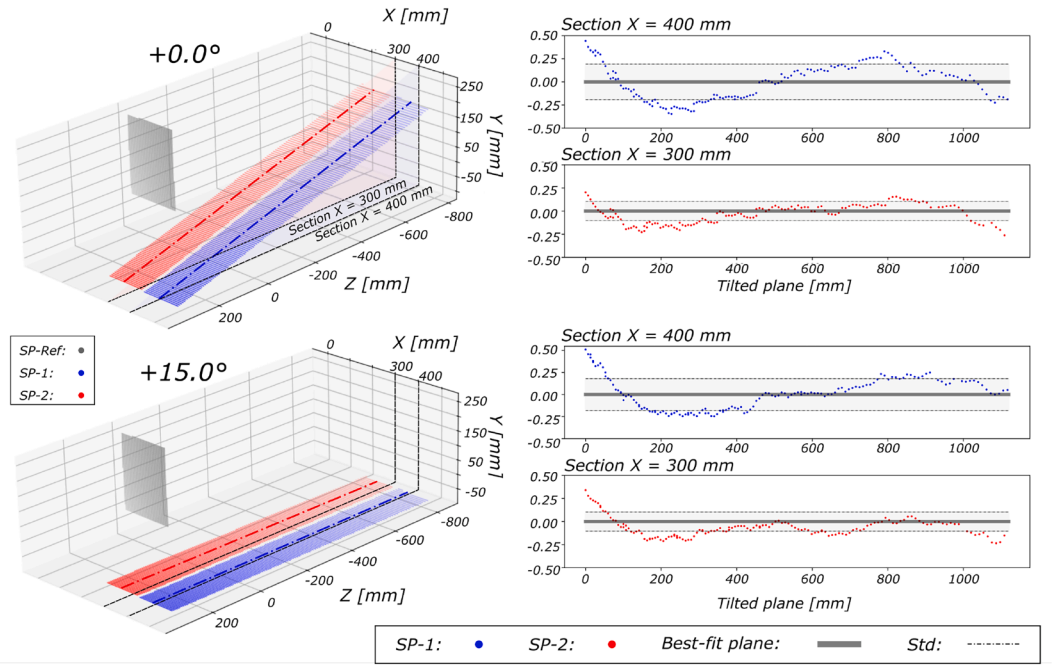

Fig. 11. 3D plots of the spatial coordinates of the data-points from SP-1 and SP-2 at the increments +0.0° and +15.0°. Section views at $X = 400$ and $X = 300$: SP-2 shows results that are closer to the best-fit plane with a smaller deviation compared to SP-1.

the anamorphic transformation in maintaining low uncertainties across the field.

Fig. 12 presents comprehensive σ_{pixel} measurements across the field of view for varying camera incidence angles γ. An increase of 5° in incidence roughly corresponds to a shift of two increments of 2.5° for the same anamorphic transformation. For example, an incidence angle of $\gamma = 80°$ at +15.0° is comparable to $\gamma = 85°$ at +10.0° or $\gamma = 90°$ at +5.0°. In cases of excessively high incidence, such as $\gamma = 80°$ at +12.5° and +15.0°, the DIC algorithm fails to correlate, resulting in a loss of subset center tracking.

SP-2 was generated based on a reference tilt angle of 70°. Small deviations from this reference angle during experiments–analogous to minor changes in camera incidence–introduce only slight variations in the local speckle projection. Consequently, SP-2 maintains its robustness, preserving low uncertainties across the field. If the pattern had been generated for a different reference angle, for example 60°, the effect would be equivalent to a moderate change in camera incidence, and the transformation could still be applied with minor adjustments. This highlights both the robustness of SP-2 to variations in plane tilt or camera incidence and the flexibility of the method for planar surfaces, with potential extension to more complex geometries.

4. Discussion

4.1. Benefits of the anamorphic speckle pattern

The application of the anamorphic speckle pattern to DIC has shown significant promise in enhancing measurement accuracy, particularly for LOVTAs. While effective in many scenarios, regular speckle patterns are inherently sensitive to perspective effects when applied to large or highly tilted surfaces. As illustrated in Fig. 2, increasing viewing angles induce apparent variations in speckle size, shape, and contrast across the field of view, leading to spatially non-uniform image textures.

From a feature-matching standpoint, DIC accuracy is directly governed by the quality of the correlation between subsets extracted from the reference and deformed images. Correlation criteria assume that the grayscale texture within each subset remains statistically similar, apart from rigid translation and small deformation. Perspective-induced effects violate this assumption by causing apparent changes in speckle size and shape across the image. In regions observed at high incidence angles, subsets progressively lose effective grayscale gradients and isotropy, which reduces correlation peak sharpness and increases matching ambiguity. This degradation directly manifests as increased displacement uncertainty σ_{pixel} and, in extreme cases, correlation failure.

The anamorphic speckle pattern addresses this limitation by compensating for geometric projection effects at the pattern design stage. By transforming the reference speckle pattern according to the camera viewing geometry and relative distances, the anamorphic approach ensures that speckle features appear with consistent size, shape, and spatial frequency in the acquired images. Consequently, the statistical properties of the subsets remain more uniform across the field of view, resulting in a more stable and robust correlation process. From a physical and numerical standpoint, this improvement can be interpreted through the conditioning of the DIC optimization problem. In subset-based DIC, displacement estimation relies on minimizing a correlation criterion whose local behavior is governed by the Hessian matrix of the grayscale intensity field. This Hessian matrix is constructed from spatial intensity gradients within each subset and directly controls both the sharpness of the correlation peak and the sensitivity of the solution to image noise. Strong and isotropic grayscale gradients lead to a well-conditioned Hessian matrix, whereas degraded or anisotropic textures result in poor conditioning and increased displacement uncertainty.

Perspective effects inherent to regular speckle patterns cause apparent variations in speckle size and shape across the image, particularly for large fields of view and oblique viewing angles. In highly tilted regions, speckles appear compressed along one direction and blurred along another, reducing effective gradient content and introducing anisotropy within the subsets. This directly degrades the conditioning of the Hessian matrix, broadens the correlation peak, and increases sensitivity to noise and interpolation errors, which manifests as elevated σ_{pixel} values and spatially non-uniform uncertainty.

The anamorphic transformation acts as a geometric pre-compensation mechanism that restores uniform speckle appearance in

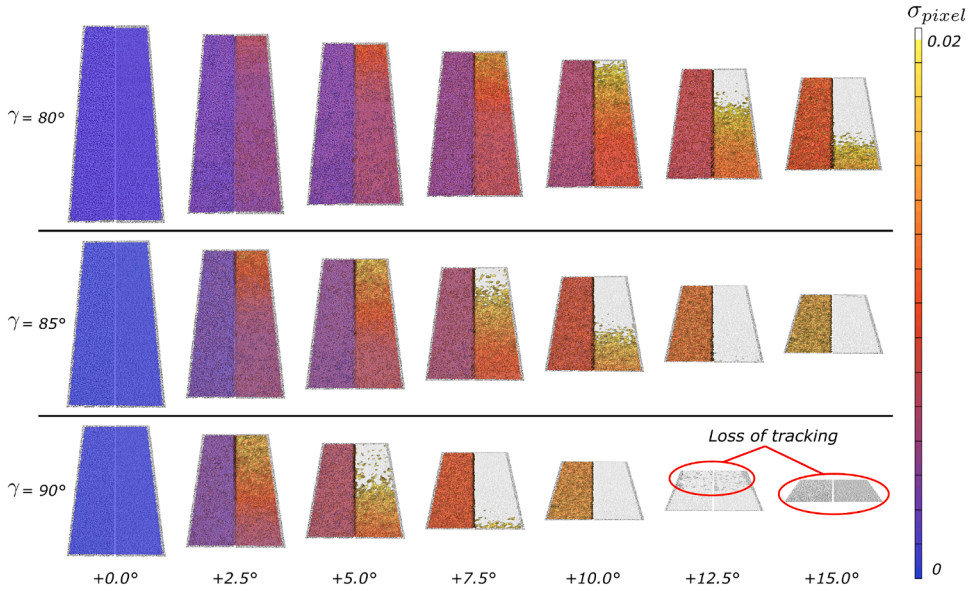

Fig. 12. Influence of the camera incidence γ on the DIC measurements with virtually generated images: An increase of 5° in the incidence angle γ approximately corresponds to a shift of two increments of 2.5° for the same anamorphic transformation. Overall, the distribution σ_{pixel} increases as the incidence γ increases. SP-2 provides a lower uncertainty over SP-1.

the image plane. By adjusting the spatial distribution of the speckle pattern prior to imaging, the transformation ensures that speckle size, spacing, and orientation remain approximately constant after projection, regardless of local incidence angle. As a result, the grayscale gradients within each subset remain strong and isotropic over the entire field of view, leading to a better-conditioned Hessian matrix and a sharper, more stable correlation minimum. This improved numerical conditioning explains, from first principles, the observed reduction in uncertainty and the enhanced robustness of feature matching when using the anamorphic speckle pattern. This behavior is confirmed experimentally, as the anamorphic pattern consistently produces lower σ_{pixel} values, as shown in Figs. 8, 9, and 12. In contrast, the regular speckle pattern exhibits a pronounced increase in uncertainty in regions affected by strong perspective effects.

Beyond uncertainty reduction, this improvement is also reflected in the spatial behavior of the subset centers. Fig. 11 illustrates the spatial distribution of the reconstructed subset center positions. For the regular speckle pattern, perspective-induced degradation leads to increased spatial scatter and systematic deviations of the subset centers, particularly at high incidence angles. The anamorphic pattern, however, maintains a more homogeneous and stable spatial distribution, indicating improved subset tracking consistency across the entire field of view. These combined effects–reduced uncertainty and improved spatial coherence–are particularly critical for large-scale structures, where depth variations and oblique viewpoints are unavoidable and where conventional speckle patterns struggle to provide reliable full-field measurements.

4.2. Challenges and limitations

Despite its benefits, implementing the anamorphic speckle pattern presents challenges. Designing and generating the anamorphic pattern requires understanding the viewing geometry and DIC system requirements. This process can be complex and time-consuming. Applying the anamorphic transformation requires substantial computational resources.

From a computational standpoint, the generation of the anamorphic pattern involves point-wise geometric transformations driven by camera orientation and surface descriptions. This process is performed entirely offline and therefore does not affect image acquisition or DIC computations during testing. However, for large-scale patterns or finely discretized surfaces, pattern generation may become computationally demanding. Future work could focus on algorithmic optimization, parallelization strategies, or the use of reduced surface representations to decrease generation time without compromising accuracy.

Practical implementation also poses challenges, particularly for large or complex structures. Producing and applying high-precision speckle patterns on curved or extensive surfaces may be limited by printing resolution, material handling, and surface accessibility. Techniques such as segmented pattern application, modular printing, or direct pattern deposition methods (e.g., projection or spraying guided by templates) could mitigate these constraints and improve scalability.

From a system robustness perspective, the effectiveness of the anamorphic transformation inherently depends on the accuracy of the imaging geometry used during pattern generation. Errors in camera calibration, camera pose estimation, or surface orientation may lead to imperfect geometric pre-compensation, resulting in residual variations of projected speckle size and anisotropy in the image plane. While this sensitivity is not unique to the proposed approach–since accurate calibration is already a prerequisite for stereo-DIC–the anamorphic transformation makes this dependency explicit at the pattern-design stage. For curved or large-scale structures, additional uncertainty may arise from inaccuracies in the surface description used to compute local incidence angles, particularly when relying on CAD models or photogrammetric reconstructions. In such cases, segmentation strategies and locally adaptive transformations may help limit error propagation. Consequently, once applied, the anamorphic speckle pattern can be used in the same manner as a conventional pattern, with the primary trade-off being an increased sensitivity to geometric modeling assumptions rather than changes in acquisition or analysis protocols.

Continued research should optimize the generation and application processes to further reduce computational overhead and streamline integration into existing DIC systems.

4.2.1. Practical limitations on displacement and strain measurements

The proposed anamorphic speckle pattern does not introduce any new theoretical limit on the measurable displacement or strain compared to conventional stereo-DIC. The maximum admissible displacement is still fundamentally constrained by the subset size S and the need to preserve speckle uniqueness within each subset. A common rule of thumb in DIC is that the maximum displacement should remain smaller

than the subset size, ensuring sufficient overlap for reliable correlation. This practical guideline helps maintain tracking robustness across the measurement region. Similarly, the maximum measurable strain depends on the spatial resolution defined by the subset size and step, as well as the speckle contrast and density.

The role of the anamorphic transformation is instead to mitigate perspective-induced distortions that degrade correlation quality for LOVTAs. By pre-compensating the apparent speckle deformation in the image plane, the method maintains more uniform speckle size and spacing, reducing matching uncertainty. This improvement enhances correlation robustness and measurement precision, effectively delaying the onset of decorrelation for a given subset size and camera orientation.

In the present study, only rigid-body displacements were analyzed, and no explicit upper bounds on displacements or strain were experimentally imposed. However, in typical DIC applications, the practical limits are still set by the subset size, speckle quality, and correlation parameters. The apparent speckle size may evolve during deformation due to the combined effects of imaging geometry and local mechanical strain. The proposed anamorphic transformation compensates for the initial perspective-induced distortion at the reference state, while subsequent variations are inherently captured by the correlation process as part of the measured deformation. As long as speckle features remain distinguishable within each subset, these variations will not compromise displacement tracking. Future work will extend the validation to controlled deformation tests, allowing the quantification of correlation loss thresholds and strain measurement accuracy under realistic loading conditions.

4.2.2. Practical implementation of anamorphic speckle patterns

In practical applications, the generation of an anamorphic speckle pattern relies on prior knowledge of the imaging geometry, including camera pose and surface orientation, which are already required inputs for stereo-DIC calibration. For planar or locally planar regions, as investigated in this study, the transformation is computed once from the calibrated camera configuration and applied to generate a single optimized speckle pattern. This pattern can then be produced using standard techniques such as large-format printing on adhesive films and applied to the measurement surface in the same manner as conventional speckle patterns.

For curved structures, such as wings or fuselages, the same principle can be extended by incorporating the local surface geometry into the transformation. When a surface description is available from CAD models or photogrammetric reconstruction, the anamorphic transformation can be applied locally using the surface normal and camera incidence angle. This results in a spatially varying speckle pattern designed to maintain uniform projected speckle characteristics in the image plane, analogous to texture mapping approaches commonly used in computer vision and full-scale optical measurements.

While the present experimental validation is limited to a tilted planar surface, the underlying geometric framework of the anamorphic transformation is not restricted to planar geometries. The extension to curved surfaces primarily introduces practical considerations related to surface modeling accuracy, pattern fabrication, and application, rather than fundamental methodological limitations. Addressing these aspects, including segmentation strategies and sensitivity to calibration errors, constitutes an important direction for future work.

4.3. Applications on full-scale structures

Anamorphic speckle patterns are particularly beneficial for full-scale structures, such as those in the aerospace industry. Traditional DIC methods often struggle to provide precise measurements for these complex and extensive structures due to perspective effects. However, the anamorphic speckle pattern maintains speckle point clarity and stability across perspectives, significantly enhancing DIC measurement accuracy.

The experimental setup for testing these patterns was robust and designed to replicate the viewing point of a wing from cameras at a grazing angle of view. Specifically, applying the anamorphic speckle pattern to a wing surface can enhance the precision of DIC by ensuring that the speckle points appear consistent and undistorted regardless of the viewing angle. This approach replicates the viewing perspective of a wing from a camera, addressing the challenges posed by the complex geometry and varying angles inherent in wing surfaces. Furthermore, this technique can also be applied to aircraft fuselages, which present additional challenges due to their circular shape. The anamorphic speckle pattern can effectively account for the curvature of the fuselage, ensuring that the speckle points remain consistent and accurately represent surface deformations when viewed from different angles. Additionally, in studies such as those conducted by Li et al. [14], the anamorphic speckle pattern can replace the need for pre-stretched speckle patterns. The anamorphic speckle pattern provides a more efficient and effective alternative by directly addressing the perspective effects through its design, eliminating the need for pre-stretching and simplifying the preparation process.

5. Conclusion

This study addresses the challenge of perspective-induced effects in stereo-DIC by introducing an anamorphic transformation of the speckle pattern applied at the pattern-design stage. The geometric formulation of the transformation is presented and clarified, and its implementation is validated through a controlled experimental configuration that enables a direct comparison between a conventional speckle pattern and an anamorphically transformed one under varying camera incidence angles.

The experimental results demonstrate that geometric pre-compensation of the speckle pattern leads to a consistent reduction in matching uncertainty and improved precision in the determination of the 3D positions of subset centers when large viewing angles are involved. Although the performance of the anamorphic pattern remains influenced by camera incidence, its correlation robustness systematically exceeds that of a regular speckle pattern within the investigated configuration. These findings confirm that compensating perspective effects prior to image acquisition can significantly improve DIC uncertainty characteristics without modifying the correlation procedure itself.

The scope of the present work is intentionally focused on isolating the effect of perspective distortions and evaluating the contribution of speckle pattern design under controlled rigid-body motion on a planar surface. This planar configuration provides a repeatable and well-defined framework for assessing correlation robustness independently of additional sources of variability such as material deformation, complex curvature, or operational constraints. The aim is methodological: to establish the transformation framework and demonstrate its practical implementation in a controlled setting. While the anamorphic transformation is formulated within a general geometric framework and can be extended analytically or numerically to curved or free-form surfaces when their geometry is known, experimental validation in this manuscript is deliberately limited to the planar case to provide a clear baseline for future studies.

From a practical standpoint, the computational cost associated with the anamorphic transformation is confined to an offline preprocessing step during speckle pattern generation and does not affect the DIC correlation or experimental workflow. Nevertheless, applying high-precision speckle patterns to large or complex structures may be constrained by printing resolution, surface accessibility, and geometric modeling accuracy. The effectiveness of the geometric pre-compensation also depends on the accuracy of the calibrated imaging geometry, a requirement that remains consistent with standard stereo-DIC practice. Within these boundaries, the present study establishes the feasibility and benefit of geometric pre-compensation for LOVTAs. It provides a foundation

for future investigations addressing curved geometries, full-scale structures, and operational measurement conditions.

CRediT authorship contribution statement

Stéphane W. Hu: Writing – review & editing, Writing – original draft, Visualization, Validation, Supervision, Project administration, Methodology, Investigation, Formal analysis, Data curation, Conceptualization; **Guilhem Marchal:** Software, Investigation, Data curation; **Yvan Dilem:** Software, Investigation, Data curation; **Denis Walch:** Writing – review & editing, Supervision, Project administration, Funding acquisition; **Ilyass Tabiai:** Writing – review & editing, Supervision, Resources, Project administration, Funding acquisition, Conceptualization.

Data availability

The data and code are linked in the paper

Declaration of competing interest

The authors declare the following financial interests/personal relationships which may be considered as potential competing interests:

Stéphane W. Hu reports financial support was provided by Bombardier Inc. If there are other authors, they declare that they have no known competing financial interests or personal relationships that could have appeared to influence the work reported in this paper.

Supplementary material

Supplementary material associated with this article can be found in the online version at 10.1016/j.optlaseng.2026.109773.

References

[1] North Atlantic Treaty Organization, Research and Technology Organization, Introduction to flight test engineering = Introduction aux techniques des essais en vol. North Atlantic Treaty Organisation, Research & Technology Organisation; 2005. OCLC: 61490642.

[2] Norton WJ. Structures flight test handbook:. Defense Technical Information Center; 1990. https://doi.org/10.21236/ADA257262

[3] Rouse M, Jegley D, McGowan D, Bush H, Waters W, et al. Utilization of the building-block approach in structural mechanics research. In: 46th structures, structural dynamics and materials conference. American Institute of Aeronautics and Astronautics. ISBN 978-1-62410-065-9; 2005, p. 1. https://doi.org/10.2514/6.2005-1874

[4] Stoliker FN. Introduction to flight test engineering: = (Introduction à la technique d'essais en vol). No. 14 = 300 [des Gesamtw.] in AGARDograph Flight test techniques series; AGARD; 1995. ISBN 978-92-836-1020-5.

[5] Richards L. Research and Technology Organization, Flight Test Technology Team, Application of fiber optic instrumentation RTO-AG-160-V22 (SCI 228) ; AC/323(SCI-228)TP/446 = validation des systemes d'instrumentation par fibres optiques. Research and Technology Organization, North Atlantic Treaty Organization; 2012. note: 9789283701644 Place: Neuilly-sur-Seine OCLC: 930929408.

[6] Sutton MA, Yan JH, Tiwari V, Schreier HW, Orteu JJ, et al. The effect of out-of-plane motion on 2d and 3d digital image correlation measurements. Opt Laser Eng 2008;46(10):746–57. https://doi.org/10.1016/j.optlaseng.2008.05.005

[7] Canal LP, González C, Molina-Aldareguía JM, Segurado J, LLorca J, et al. Application of digital image correlation at the microscale in fiber-reinforced composites. Compos Part A: Appl Sci Manufact 2012;43(10):1630–8. https://doi.org/10.1016/j.compositesa.2011.07.014

[8] Lee CH, Salit MS, Hassan MR, et al. A review of the flammability factors of kenaf and allied fibre reinforced polymer composites. Adv Mater Sci Eng 2014;2014:1–8. https://doi.org/10.1155/2014/514036

[9] Wang B, Pan B. Subset-based local vs. finite element-based global digital image correlation: a comparison study. Theor Appl Mech Lett 2016;6(5):200–8. https://doi.org/10.1016/j.taml.2016.08.003

[10] Tabiai I, Tkachev G, Diehl P, Frey S, Ertl T, Therriault D, et al., et al. Hybrid image processing approach for autonomous crack area detection and tracking using local digital image correlation results applied to single-fiber interfacial debonding. Eng Fract Mech 2019;216:106485. https://doi.org/10.1016/j.engfracmech.2019.106485

[11] Chu TC, Ranson WF, Sutton MA, et al. Applications of digital-image-correlation techniques to experimental mechanics. Exp Mech 1985;25(3):232–44. https://doi.org/10.1007/BF02325092

[12] Song H, Liu C, Zhang H, Leen S, et al. A DIC-based study on fatigue damage evolution in pre-corroded aluminum alloy 2024-t4. Mater (Basel) 2018;11(11):2243. https://doi.org/10.3390/ma11112243

[13] Sutton MA, Orteu J-J, Schreier H, et al. Image correlation for shape, motion and deformation measurements. Springer US; 2009. ISBN 978-0-387-78746-6 978-0-387-78747-3. https://doi.org/10.1007/978-0-387-78747-3

[14] Li L-G, Liang J, Guo X, Guo C, Hu H, Tang Z-Z, et al. Full-field wing deformation measurement scheme for in-flight cantilever monoplane based on 3d digital image correlation. Meas Sci Technol 2014;25(6):065202. https://doi.org/10.1088/0957-0233/25/6/065202

[15] Stéphane W. H, Alessandra L, Jacques L, Martin L, Daniel T, Denis W, et al., Full-field measurements applied to the experimental testing of structural parts for the aerospace industry. In: Canadian Society for Mechanical Engineering Congress - CSME 2021. 2021, p. 1. https://www.researchgate.net/publication/353886933_Full-field_measurements_applied_to_the_experimental_testing_of_structural_parts_for_the_aerospace_industry. https://doi.org/10.13140/RG.2.2.29642.29129

[16] Reu PL, Sutton M, Wang Y, Miller TJ, et al. Uncertainty quantification for digital image correlation. In: Office of scientific and technical information. 2009, p. 7. https://www.osti.gov/biblio/1142312.

[17] Genovese K, Chi Y, Pan B, et al. Stereo-camera calibration for large-scale DIC measurements with active phase targets and planar mirrors. Opt Express 2019;27(6):9040. https://doi.org/10.1364/OE.27.009040

[18] Peng B. Modified correlation criterion for digital image correlation considering the effect of lighting variations in deformation measurements. Opt Eng 2012;51(1):017004. https://doi.org/10.1117/1.OE.51.1.017004

[19] Wang YQ, Sutton MA, Bruck HA, Schreier HW, et al. Quantitative error assessment in pattern matching: effects of intensity pattern noise, interpolation, strain and image contrast on motion measurements. Strain 2009;45(2):160–78. https://doi.org/10.1111/j.1475-1305.2008.00592.x

[20] Wieneke B, Prevost R. DIC Uncertainty estimation from statistical analysis of correlation values. In: Jin H, Sciammarella C, Yoshida S, Lamberti L, editors. Advancement of optical methods in experimental mechanics, volume 3. Springer International Publishing. ISBN 978-3-319-00767-0 978-3-319-00768-7; 2014, p. 125–36. Series Title: Conference Proceedings of the Society for Experimental Mechanics Series; https://doi.org/10.1007/978-3-319-00768-7

[21] Wang D, DiazDelaO FA, Wang W, Lin X, Patterson EA, Mottershead JE, et al. Uncertainty quantification in DIC with kriging regression. Opt Lasers Eng 2016;78:182–95. https://doi.org/10.1016/j.optlaseng.2015.09.006

[22] Balcaen R, Reu PL, Lava P, Debruyne D, et al. Stereo-DIC uncertainty quantification based on simulated images. Exp Mech 2017;57(6):939–51. https://doi.org/10.1007/s11340-017-0288-9

[23] Dong YL, Pan B. A review of speckle pattern fabrication and assessment for digital image correlation. Exp Mech 2017;57(8):1161–81. https://doi.org/10.1007/s11340-017-0283-1

[24] Li Y, Zhao J, Zhou J, Yang Y, Huang X, Liu Z, et al. Local-micro-zone-wise time-resolved integrated digital image correlation for evaluating the mechanical properties of welding joints. Exp Tech 2023;47(5):973–87. https://doi.org/10.1007/s40799-022-00608-y

[25] Huang Y, Huang X, Zhong M, Liu Z, et al. A bilayer color digital image correlation method for the measurement of the topography of a liquid interface. Opt Laser Eng 2023;160:107242. https://doi.org/10.1016/j.optlaseng.2022.107242

[26] Hou X, Zeng D, Huang X, Zhang H, Liu Z, Huang X, et al. Study on the long-term monitoring of contact deformation field of periodic rotating gears using DIC combined with SURF algorithm. Exp Mech 2025;65(7):1055–68. https://doi.org/10.1007/s11340-025-01189-8

[27] Sanchez-Reyes J, Chacan JM. Anamorphic free-form deformation. Comput Aid Geom Des 2016;46:30–42. https://doi.org/10.1016/j.cagd.2016.06.002